Supporting Information

Chatre et al. 10.1073/pnas.1422264112

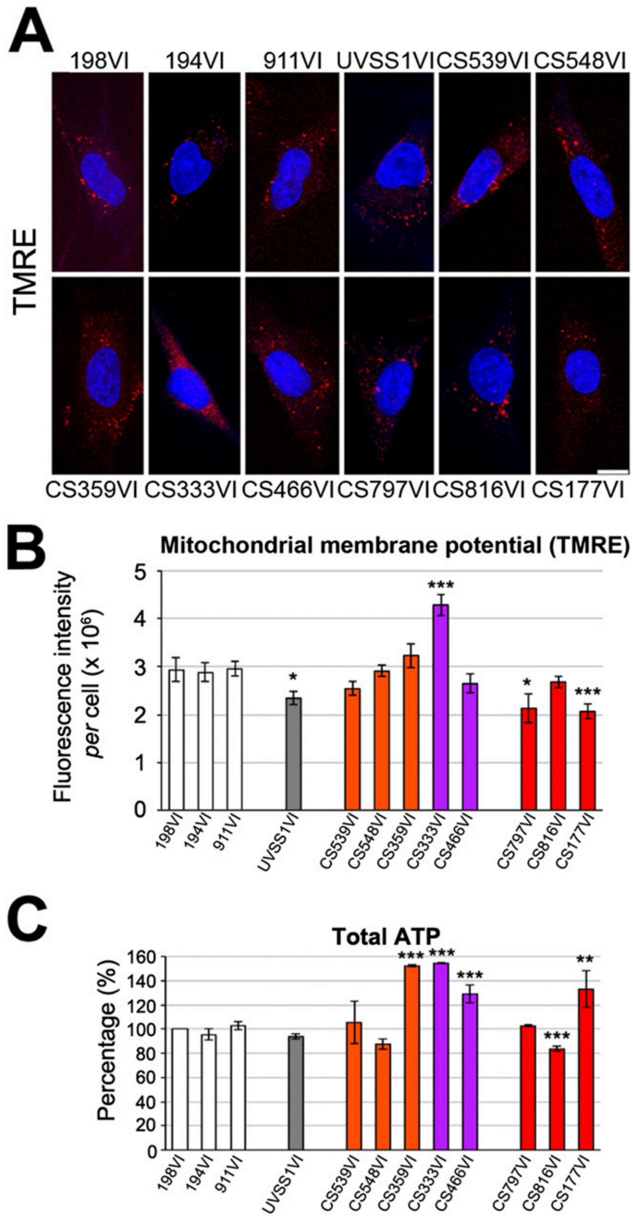

Fig. S1. TMRE and ATP measurements in primary controls, CS and UV^{S}S patient cells. (*A*) 3D reconstructions of TMRE-treated cells (red) counterstained with Hoechst (blue). (Scale bar: 10 μm.) (*B*) Quantification of TMRE. $n = 30$ cells from three independent experiments, mean ± SEM. (*C*) Total ATP levels per 10,000 cells, expressed as a percentage of control (100%); $n = 3$ independent experiments; mean ± SD $*P \leq 0.05$, $**P \leq 0.01$, $***P \leq 0.001$ versus control 198VI cells, based on the unpaired *t* test.

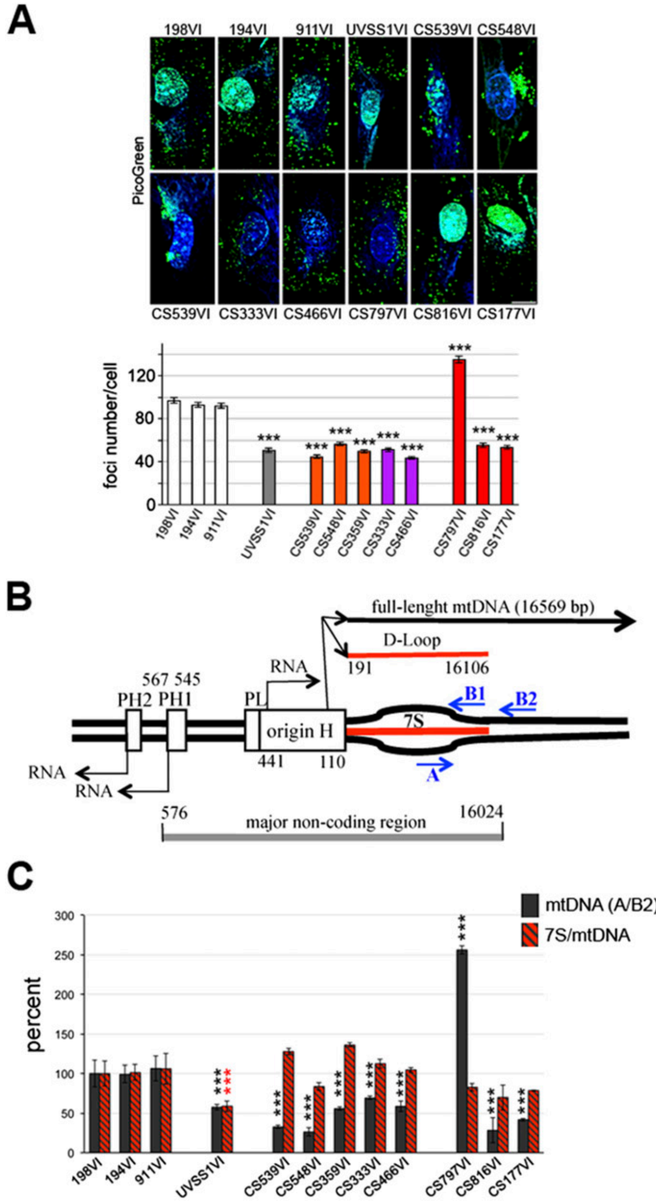

D

	198VI	194VI	911VI		UVSS1VI		CS539VI	CS548VI	CS359VI	CS333VI	CS466VI		CS797VI	CS816VI	CS177VI
POLG1/POLG2	1.99	1.74	1.84		2.00		0.35	0.20	1.05	0.61	0.86		0.13	0.24	0.06

Fig. S2. Alterations in mitochondrial DNA in patient-derived fibroblasts. (*A*) Quantitation of mtDNA by PicoGreen staining that detects double-stranded DNA in nucleoids (1, 2). (*Upper*) 3D reconstructions of primary fibroblasts from UV^{S}S and CS patients and from healthy controls stained with PicoGreen. (*Lower*) Cytoplasmic Picogreen labeled entities were enumerated per cell. $n = 30$ cells from three independent experiments per condition. ***$P \leq 0.001$ versus control 198VI cells, based on the unpaired *t* test. (*B*) Schematic representation (not to scale) of the human mtDNA regulatory region and the relative RNA and DNA products. Mitochondrial genetic elements are shown (PH1-PH2: promoters of the H strand; PL: promoter of the L-strand; Origin H: origin of the H strand, etc.) with key coordinates. DNA replication can result in either an abortive DNA sequence (7S DNA, 654 nt in length), which forms a triple strand with the template DNA, or a full-length mtDNA. In blue are indicated the primers A (coordinates: 16259–16240), B1 (16128–16108), and B2 (16055–16036) used for estimation of 7S DNA and mtDNA content by real-time qPCR, as described (3). Primers A/B1 amplify a region within the 7S, which includes abortive 7S molecules and longer size mtDNA. Primers A/B2 amplify longer-size mtDNA. The 7S DNA is evaluated as (A/B1) – (A/B2). (*C*) mtDNA resulted here from amplification with the pair A/B2. The 7S/mtDNA ratio was 1.98 ± 027 in primary fibroblasts from healthy individuals tested in this study. Alterations in mtDNA content (region A/B2, black columns) and in the 7S/mtDNA ratio (hatched red) were compared with the control, 198VI (considered 100%). Note that both values are stable among control cells, reduced in the UV^{S}S cells, and highly divergent toward each other in CS fibroblasts. ***$P \leq 0.001$, based on unpaired *t* test comparisons of cells versus control 198VI. Black stars: mtDNA; red stars 7S/mtDNA, versus the respective controls. (*D*) Ratio of POLG1/POLG2 fluorescence intensity for cells of each individual (absolute values are from quantification of POLG1 in Fig. 1*E* and POLG2 in Fig. 1*G*). Note that control and UVS^{S}1 cells display a 1.65- to 25-fold higher value than CS cells.

1. Ashley N, Harris D, Poulton J (2005) Detection of mitochondrial DNA depletion in living human cells using PicoGreen staining. *Exp Cell Res* 303(2):432–446.
2. He J, et al. (2005) The AAA+ protein ATAD3 has displacement loop binding properties and is involved in mitochondrial nucleoid organization. *J Cell Biol* 176(2):141–146.
3. Chatre L, Ricchetti M (2013) Prevalent coordination of mitochondrial DNA transcription and initiation of replication with the cell cycle. *Nucleic Acids Res* 41(5):3068–3078.

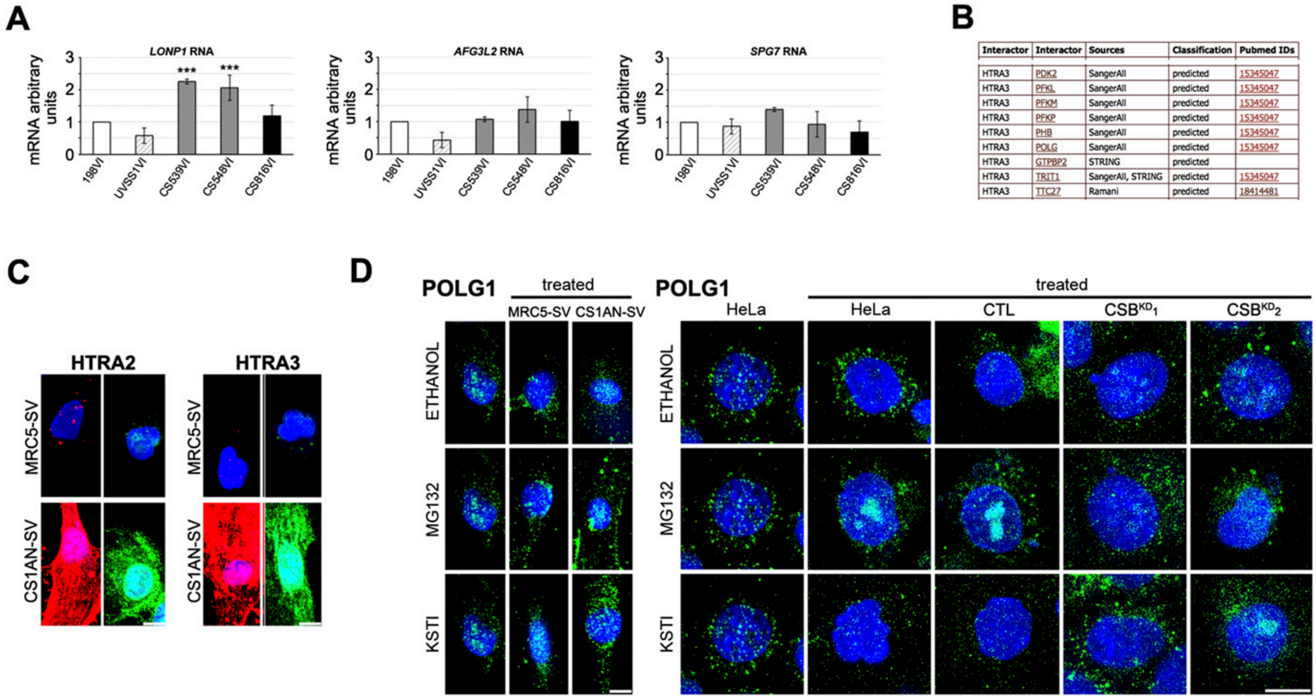

Interactor	Interactor	Sources	Classification	Pubmed IDs
HTRA3	PDK2	SangerAll	predicted	15345047
HTRA3	PFKL	SangerAll	predicted	15345047
HTRA3	PFKM	SangerAll	predicted	15345047
HTRA3	PFKP	SangerAll	predicted	15345047
HTRA3	PHB	SangerAll	predicted	15345047
HTRA3	POLG	SangerAll	predicted	15345047
HTRA3	GTPBP2	STRING	predicted	
HTRA3	TRIT1	SangerAll, STRING	predicted	15345047
HTRA3	TTC27	Ramani	predicted	18414481

Fig. S3. Serine-protease inhibitors restore original parameters in patient-derived CS cells and CSB–impaired cells. (*A*) Quantitative RT-qPCR of the *LONP1* (Lon protease), *AFG3L2* (AAA protease), and *SPG7* (paraplegin) mRNAs in some control and patient-derived cells. $n = 3$ independent experiments, mean ± SD ***$P \leq 0.001$, based on unpaired *t* test comparisons of patient cells versus control 198VI. (*B*) Table of HTRA3 interactions, according to the Prion Disease Database, PDDB (prion.systemsbiology.net/page/Welcome/display), with interactors listed in the first two rows, the sources of the interaction in the third row, classification of interaction as empirical or predicted in the fourth row, and PubMed IDs in the last row (for HTRA3, data originated from ref. 1). PDDB predicts protein–protein interactions based on a large set of data, from two-hybrids based maps to genetic-based interaction maps. Only a few search results, including POLG (=POLG1), are shown. (*C*) 3D reconstructions of (*Upper*) MRC5-SV and (*Lower*) CS1AN-SV immortalized cells immunostained for (*Left*) HTRA2 or (*Right*) HTRA3, and counterstained with Hoechst (blue). Secondary antibodies were inverted compared with Fig. 3 *E* and *F*. Both Alexa Fluor 555 (red) and Alexa Fluor 488 (green) conjugated secondary antibodies showed a dramatically higher signal in CS1AN-SV than in MRC5-SV, confirming results in Fig. 3 *E* and *F*. (*D*) 3D reconstructions of cells treated or untreated with the indicated compounds, immunostained for POLG1 (green), and counterstained with Hoechst (blue) in CSB cellular models: immortalized fibroblasts (*Left*), HeLa cells (*Right*). Fluorescence quantifications are shown in Fig. 4 *C* and *D*.

1. Lehner B, Fraser AG (2004) A first-draft human protein-interaction map. *Genome Biol* 5(9):R63.

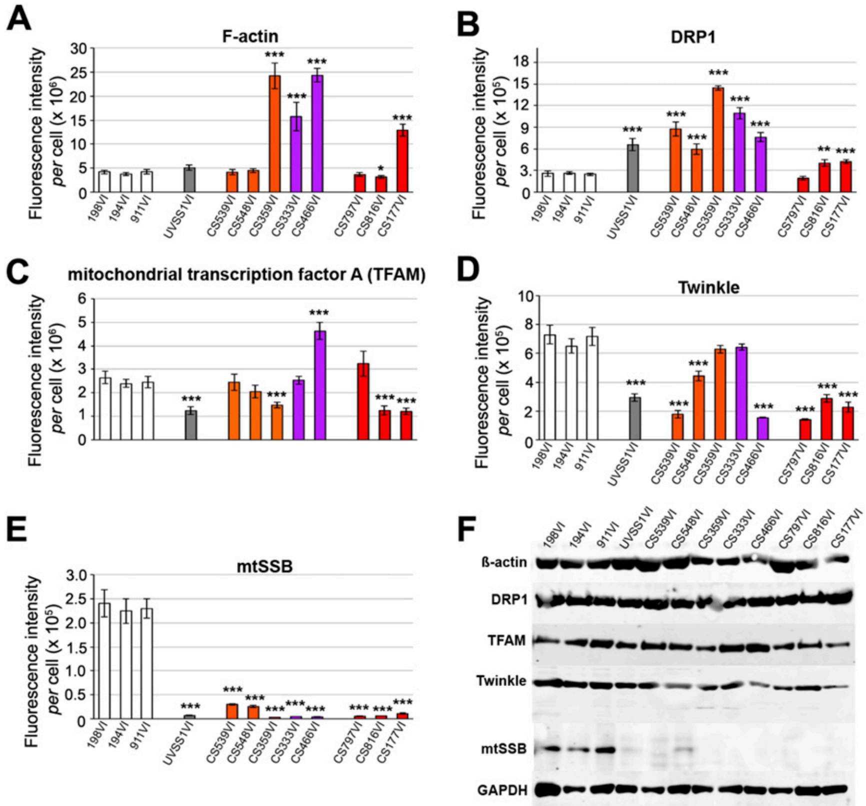

Fig. S4. Levels of cytoplasmic and mitochondrial proteins in fibroblasts from patients with UV^{S}S and CS. (*A*) Fluorescence intensity quantification of cytoplasmic F-actin (filamentous actin, a linear polymer) by rhodamine-falloidin fluorescence staining. Fluorescence intensity quantification of mitochondrial proteins: DRP1 (*B*), TFAM (*C*), Twinkle (*D*), and mtSSB (*E*) by immunolabeling. $n = 30$ cells from three independent experiments; mean ± SEM $***P \leq 0.001$, $**P \leq 0.01$, $*P \leq 0.05$ versus 198VI, based on the *t* test. (*F*) Immunoblot of β-actin (Abcam), DRP1 (Santa Cruz), TFAM (Santa Cruz), Twinkle (Abcam), mtSSB (Abcam), and GAPDH (Santa Cruz) loading control from whole-cell extracts. Note that rhodamine-phalloidine fluorescence stains filamentous actin (F-actin), a linear polymer, and the β-actin antibody recognizes denaturated actin, which includes the filamentous and globular (momomeric) form of the protein.

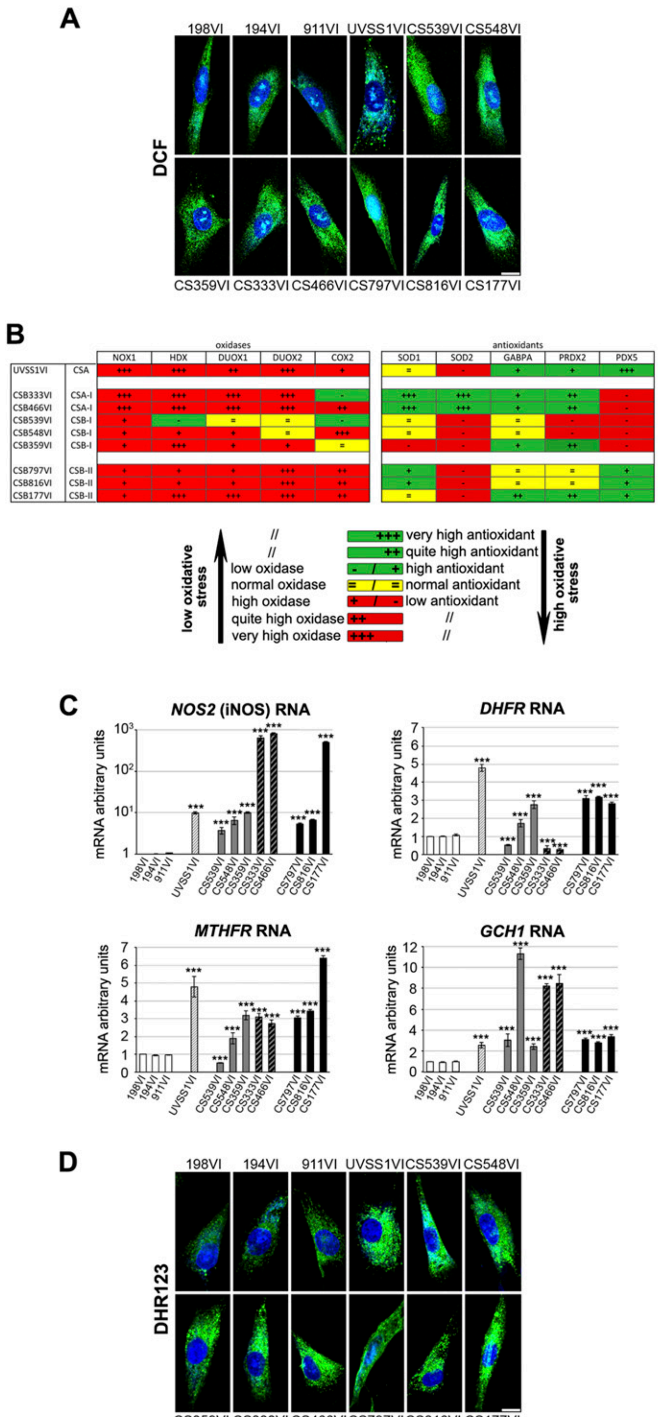

Fig. S5. Expression of oxidases and antioxidant factors in patient-derived CS fibroblasts. (*A*) 3D reconstructions of cells treated with DCFDA to detect ROS levels. ROS produced DCF (green) from DCFDA, and cells were counterstained with Hoechst (blue). Quantifications are shown in Fig. 5*A*. (*B*) Analytic representation of the expression of (*Upper Left*) oxidant factors and (*Upper Right*) antioxidant in patient-derived cells compared with controls. =, no difference; + to +++, increased expression; −, decreased expression. (*Lower*) Color coding for the effects of expression. (*C*) Quantitative RT-qPCR of factors involved in NO production: constitutive endothelial nitric oxide synthase NOS2/iNOS, and DHFR, MTHFR, and GCH1 that are involved in the biosynthesis and recycling of NO-producing cofactor BH4 (y = log scale for iNOS). $n = 3$ independent experiments, mean ± SD. (*D*) 3D reconstructions of DHR123-treated cells for detecting peroxynitrite levels (green), and counterstaining with Hoechst (blue). Quantifications are shown in Fig. 5*E*. (Scale bar: 10 μm.) $^{***}P \leq 0.001$ versus the respective controls, based on unpaired *t* tests.

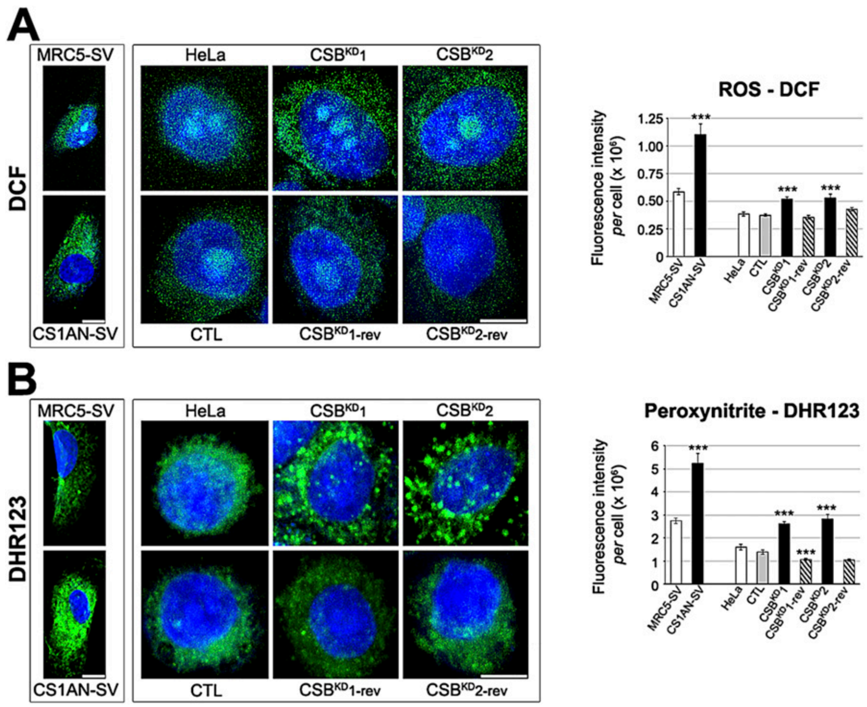

Fig. S6. Oxidases and antioxidant factors in CSB-impaired cells. (*A*) (*Left*) 3D reconstructions of cells treated with DCFDA to detect ROS levels (green) and counterstained with Hoechst (blue). (*Right*) Quantification of DCF fluorescence intensity per cell. (*B*) (*Left*) 3D reconstructions of cells treated with DHR123 (green) to detect peroxynitrite levels and counterstained with Hoechst (blue). (*Right*) Quantification of DHR123 fluorescence intensity per cell. (Scale bar: 10 μm.) Immunofluorescence, $n = 30$ cells from three independent experiments, mean ± SEM; $***P \leq 0.001$ versus controls, based on unpaired *t* tests.

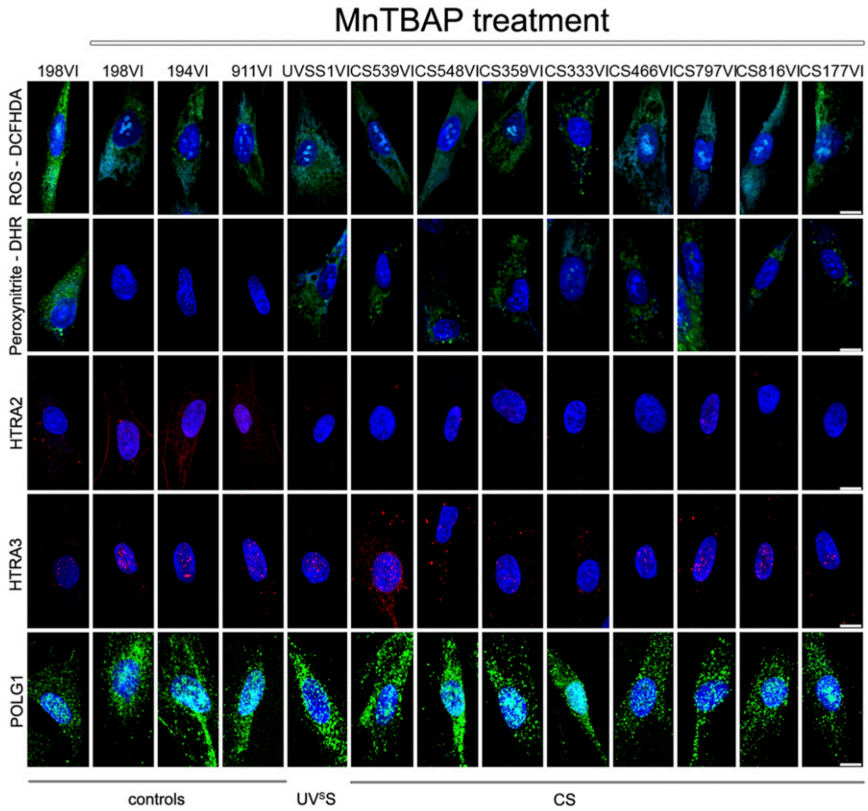

Fig. S7. Imaging of MnTBAP treatment in primary fibroblasts. 3D reconstructions of cells treated with DCFDA (green) to detect ROS levels (top row); treated with DHR123- (green) to detect peroxynitrite levels (second row); or immunostained with HTRA2 (red, third row), HTRA3 (red, fourth row), or POLG1 (green, bottom row). Cells are primary fibroblasts derived from healthy individuals (columns 1–4), patient with UV^{S}S (column 5), or patients with CS (columns 6–13) . All samples were counterstained with Hoechst (blue) to identify the nucleus. Cells were untreated (198VI control) or treated (horizontal bar) with 5 μM MnTBAP for 5 h. Fluorescence quantifications of these samples are shown in Fig. 6 *A*–*E*.

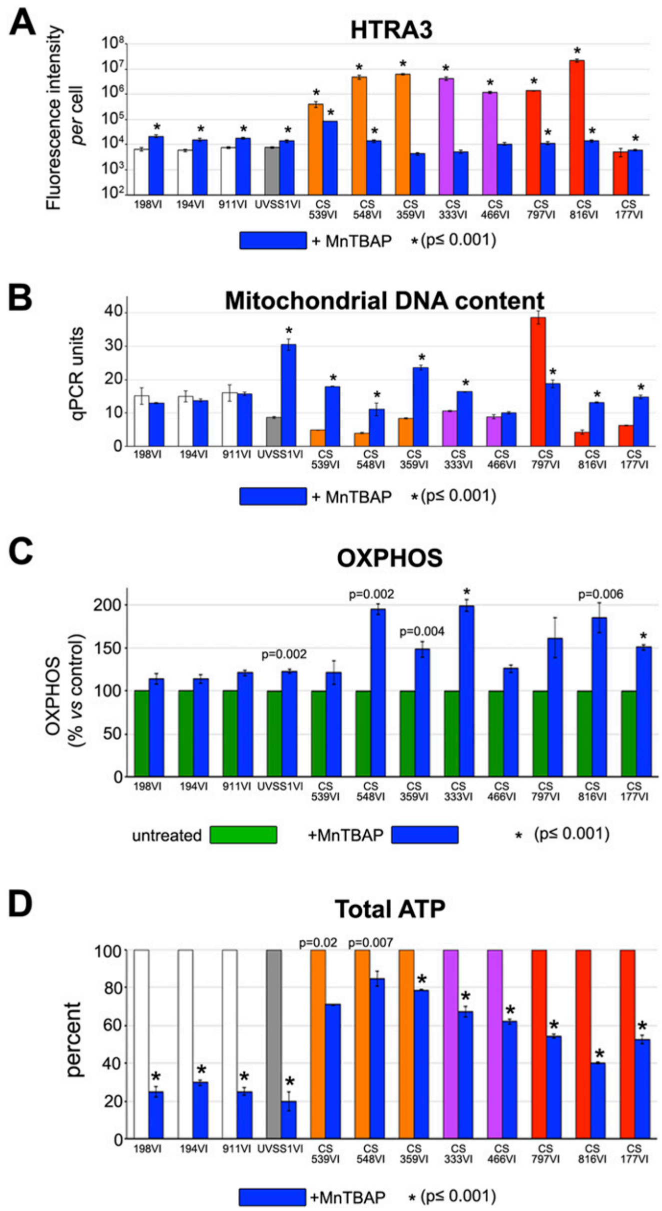

Fig. S8. Quantification of MnTBAP treatment in primary fibroblasts. (*A*) Quantifications of fluorescence intensities per cell for HTRA3, mean ± SEM $^*P \leq 0.001$ versus 198VI, based on *t* tests. Absolute values of fluorescence intensity per cell (from Fig. 6*D*) are shown here. Note that upon MnTBAP treatment CS359VI, CS333VI, and CS466VI cells restored HTRA3 levels as in healthy control cells. (*B*) qPCR results show mtDNA content (12S). Note that in the presence of MnTBAP the mtDNA content increased in patient cells that originally had low contents, but decreased in the CS797VI cells that originally had high content. Values are from Fig. 6*F*. (*C*) OXPHOS (oligomycin-sensitive) activity in ATP synthesis; results for samples treated with MnTBAP are shown in blue; results for controls (normalized to 100%) are in green. (*D*) Total ATP levels per 10,000 cells, expressed as a percentage of the respective untreated control. Immunofluorescence, $n = 30$ cells from three independent experiments, mean ± SEM qPCR and ATP measurements, $n = 3$ independent experiments, mean ± SD. MnTBAP-treated versus the respective untreated control, based on *t* tests. $^*P \leq 0.001$ versus 198VI, based on *t* tests. Other significant *P* values are indicated on top of the respective column in *C* and *D*.

Table S1. Genes, sequences of primers, and related references used in this study

Gene	Forward	Reverse	Reference
RT-qPCR primers			
TBP	CTCACAGGTCAAAGGTTTAC	GCTGAGGTTGCAGGAATTGA	1
NRF1	GGAGTGATGTCCGCACAGAA	CGCTGTTAAGCGCCATAGTG	2
NRF2a	CAGCCTGAACTGGTTGCACA	TCAACTCCGCTGCACTGTAT	3
PARKIN	GGCTGGCTGTCATTCTGCAC	TCCCGGCTGCACTCTTTGAC	4
PINK1	GGACGCTGTTCCTCGTTA	ATCTGCGATCACCAGCCA	5
PGC1a	TGTGCTGCTCTGGTTGGTG	GCTGAGTGTTGGCTGGTGC	6
SOD1	GGTGGGCCAAAGGATGAAGA	GGCGATCCCAATTACACCAC	7
SOD2	CCTCCCCGACCTGCCCTACG	TCTCCCTTGGCCAACGCCTC	7
Catalase	ACTGGGATCTCGTTGGAAAT	CCCCCGATCACTGAACAAGA	7
PRXD2	CCAGACGCTTGTCTGAGGAT	ACGTTGGGCTTAATCGTGTC	8
PRXD5	CCCTGGATGTTCCAAGACAC	AAGATGGACACCAGCGAATC	8
NOX1	TTGTTTGGTTAGGGCTGAATGT	GCCAATGTTGACCCAAGGATTTT	9
DUOX1	GCAGCGATTTGATGGGTGGTA	AGGTGGGGTTCTCCCAAGG	9
DUOX2	CTGGGTCCATCGGGCAATC	GTCGGCGTAATTGGCTGGTA	9
XDH	ACCCCGTGTTCATGGCCAGTG	TCCGGGAGGCCTGCTTGAATG	10
COX-1	AGAAACAACAGGGGAAACTA	AAGAAAGGACAGGACACAAG	11
COX-2	AAGTCCCTGAGCATCTACGGTTT	GTTGTGTTCCCTCAGCCAGATT	11
TFB1M	GGACACTCGATTTATTCCTG	ACATCTCCATGAACAATTCT	3
TFB2M	TCTGGCAATTAGCTTGTGAG	CCTACGCTTTGGGTTTTCCA	3
POLRMT	GACATGTACAACGCCGTGAT	AGCCGGCATCCTTCACCATG	3
16S	GTATGAATGGCTCCACGAGG	GGTCTTCTCGTCTTGCTGTG	12
CYTB	CTCCCGTGAGGCCAAATATC	GAATCGTGTGAGGGTGGGAC	12
HTRA2	TTTGCCATCCCTTCTGATCG	ACACCATGCTGAACATCGGG	This paper*
HTRA3-S	GAGGGCTGGTCACATGAAGA	GCTCCGCTAATTTCCAGT	13
HTRA3-L	ATGCGGACGATCACACCAAG	CGCTGCCCTCCGTTGTCTG	13
POLG	GAGAAGGCCCAGCAGATGTA	ATCCGACAGCCGATACCA	14
iNOS/NOS2	GACTTCTGTGACCTCCA	GGTGATGCTCCCAGACAT	15
eNOS/NOS3	GCGGCTGCATGACATTGAG	GTCGCGGTAGAGATGGTCAAGT	16
GCH1	TTGGTTATCTTCCTAACAAG	GTGCTGGTCACAGTTTTGCT	17
MTHFR	GAAGTACGAGCTCCGGGTTA	AAGATGCCCCAAGTGACAG	18
DHFR	GTTCCTGGGAGCACCTTTTC	ATGCAGACAGTGCCAGCTC	19
HIF1a	CCATTAGAAAGCAGTTCCGC	TGGGTAGGAGATGGAGATGC	20
qPCR primers			
18S	GAGAAACGGCTACCACATCC	GCCTCGAAAGAGTCCTGTAT	12
12S	GCTCGCCAGAACACTACGAG	CAGGGTTTGCTGAAGATGGC	21
A	GCTCGCCAGAACACTACGAG		22
B1		CAGCCACCATGAATATTGTAC	22
B2		GAAGCAGATTTGGGTACCAC	22

*Primers were selected using the Primer3 (primer3.ut.ee/) and Integrated DNA technologies (IDTDNA) (eu.idtdna.com/primerquest/home/index) realTime PCR softwares.

1. Mercy L, et al. (2005) Mitochondrial biogenesis in mtDNA-depleted cells involves a Ca2+-dependent pathway and a reduced mitochondrial protein import. *FEBS J* 272(19):5031–5055.
2. Savagner F, et al. (2003) PGC-1-related coactivator and targets are upregulated in thyroid oncocytoma. *Biochem Biophys Res Commun* 310(3):779–784.
3. Karamanlidis G, et al. (2010) Defective DNA replication impairs mitochondrial biogenesis in human failing hearts. *Circ Res* 106(9):1541–1548.
4. West AB, et al. (2004) N-myc regulates parkin expression. *J Biol Chem* 279(28):28896–28902.
5. Gegg ME, Cooper JM, Schapira AH, Taanman JW (2009) Silencing of PINK1 expression affects mitochondrial DNA and oxidative phosphorylation in dopaminergic cells. *PLoS ONE* 4(3):e4756.
6. Garnier A, et al. (2005) Coordinated changes in mitochondrial function and biogenesis in healthy and diseased human skeletal muscle. *FASEB J* 19(1):43–52.
7. Squires JE, Stoytchev I, Forry EP, Berry MJ (2007) SBP2 binding affinity is a major determinant in differential selenoprotein mRNA translation and sensitivity to nonsense-mediated decay. *Mol Cell Biol* 27(22):7848–7855.
8. Cha MK, Suh KH, Kim IH (2009) Overexpression of peroxiredoxin I and thioredoxin1 in human breast carcinoma. *J Exp Clin Cancer Res* 28:93.
9. Jones J, Estirado A, Redondo C, Bueno C, Martínez S (2012) Human adipose stem cell-conditioned medium increases survival of Friedreich's ataxia cells submitted to oxidative stress. *Stem Cells Dev* 21(15):2817–2826.
10. Ouyang X, et al. (2008) Fructose consumption as a risk factor for non-alcoholic fatty liver disease. *J Hepatol* 48(6):993–999.
11. Kiritoshi S, et al. (2003) Reactive oxygen species from mitochondria induce cyclooxygenase-2 gene expression in human mesangial cells: Potential role in diabetic nephropathy. *Diabetes* 52(10):2570–2577.
12. Suissa S, et al. (2009) Ancient mtDNA genetic variants modulate mtDNA transcription and replication. *PLoS Genet* 5(5):e1000474.
13. Nie G, et al. (2006) Serine peptidase HTRA3 is closely associated with human placental development and is elevated in pregnancy serum. *Biol Reprod* 74(2):366–374.
14. Setzer B, Lebrecht D, Walker UA (2008) Pyrimidine nucleoside depletion sensitizes to the mitochondrial hepatotoxicity of the reverse transcriptase inhibitor stavudine. *Am J Pathol* 172(3):681–690.
15. Zhang Y, Li C, Sun X, Kuang X, Ruan X (2012) High glucose decreases expression and activity of p-glycoprotein in cultured human retinal pigment epithelium possibly through iNOS induction. *PLoS ONE* 7(2):e31631.
16. Olszewska-Pazdrak B, Hein TW, Olszewska P, Carney DH (2009) Chronic hypoxia attenuates VEGF signaling and angiogenic responses by downregulation of KDR in human endothelial cells. *Am J Physiol Cell Physiol* 296(5):C1162–C1170.
17. Franscini N, Blau N, Walter RB, Schaffner A, Schoedon G (2003) Critical role of interleukin-1beta for transcriptional regulation of endothelial 6-pyruvoyltetrahydropterin synthase. *Arterioscler Thromb Vasc Biol* 23(11):e50–e53.
18. Pereira AC, et al. (2007) Dynamic regulation of MTHFR mRNA expression and C677T genotype modulate mortality in coronary artery disease patients after revascularization. *Thromb Res* 121(1):25–32.

19. Banka S, et al. (2011) Identification and characterization of an inborn error of metabolism caused by dihydrofolate reductase deficiency. *Am J Hum Genet* 88(2):216–225.
20. Gaber T, et al. (2011) Macrophage migration inhibitory factor counterregulates dexamethasone-mediated suppression of hypoxia-inducible factor-1 alpha function and differentially influences human CD4+ T cell proliferation under hypoxia. *J Immunol* 186(2):764–774.
21. Parone PA, et al. (2008) Preventing mitochondrial fission impairs mitochondrial function and leads to loss of mitochondrial DNA. *PLoS ONE* 3(9):e3257.
22. Antes A, et al. (2010) Differential regulation of full-length genome and a single-stranded 7S DNA along the cell cycle in human mitochondria. *Nucleic Acids Res* 38(19):6466–6476.